



This is a repository copy of *The potential for suppressing rail defect growth through tailoring rail thermo-mechanical properties.*

White Rose Research Online URL for this paper:
<http://eprints.whiterose.ac.uk/101390/>

Version: Accepted Version

Article:

Fletcher, D.I. orcid.org/0000-0002-1562-4655 and Sanusi, S.H. (2016) The potential for suppressing rail defect growth through tailoring rail thermo-mechanical properties. *Wear*, 366. pp. 401-406. ISSN 0043-1648

<https://doi.org/10.1016/j.wear.2016.06.022>

Reuse

This article is distributed under the terms of the Creative Commons Attribution-NonCommercial-NoDerivs (CC BY-NC-ND) licence. This licence only allows you to download this work and share it with others as long as you credit the authors, but you can't change the article in any way or use it commercially. More information and the full terms of the licence here: <https://creativecommons.org/licenses/>

Takedown

If you consider content in White Rose Research Online to be in breach of UK law, please notify us by emailing eprints@whiterose.ac.uk including the URL of the record and the reason for the withdrawal request.



eprints@whiterose.ac.uk
<https://eprints.whiterose.ac.uk/>

THE POTENTIAL FOR SUPPRESSING RAIL DEFECT GROWTH THROUGH TAILORING RAIL THERMO-MECHANICAL PROPERTIES

David I Fletcher* and Shahmir H Sanusi

Department of Mechanical Engineering, University of Sheffield, UK

* D.I.Fletcher@Sheffield.ac.uk

ABSTRACT

Thermal damage of rails can occur through brake lock-up, or traction control system failure to prevent wheel spin. In most cases the damage produced is shallow and takes the form of a “white etching layer”, usually thought to have a martensitic structure, formed as the steel is heated above its eutectoid temperature and then rapidly cooled as the wheel moves away. In many cases such layers are benign, but there is evidence of crack initiation at their interface with the sub-surface layers of the rail in “stud” defects. The metallurgical transformation during the formation of white etching layers leads to a volume change for the steel, leaving not only a transformed microstructure, but also locked-in stress. The influence of this additional locked-in stress on development of an initiated crack is studied in this paper, and the work extended to consider how alternative materials which react differently to the thermal input may offer a means to suppress crack development through locking in beneficial rather than problematic stresses.

1 INTRODUCTION

This paper presents an extension to previous research investigating thermal influence on crack growth in rails. The origin of the work is in building understanding of “stud” type defects which have been identified on railways and metros worldwide [1]. These have superficial similarities to squat defects, but are almost always associated with severe thermal input evidenced through the presence of thin (~100µm) white etching layer at the rail surface above the defects. Figure 1 shows the morphology of a typical defect of this type.

White etching layer on the rail surface can be formed either through extreme mechanical work [2] or by a thermal process [3] often due to brake lock-up, or traction control system failure to prevent wheel spin. Evidence from defects cut open for examination is that plastic damage is almost completely absent in stud defects [4], so thermal input in the generation of the WEL has been examined. Severe thermal input has three main consequences, which last over different durations: (i) temporary thermal expansion of the steel, (ii) permanent metallurgical transformation of the steel to WEL, and (iii) permanent locked-in stress produced by the change of material volume associated with the metallurgical transformation. In the previous investigation [5] only additional stress due to cause (i) was considered for its effect on stress intensity factors (SIFs) describing growth of an already initiated defect. In this paper the change of volume (cause iii) is brought in as an additional phenomena in the modelling, opening up two routes of investigation. First, taking expansion characteristic of current rail steels undergoing transformation to WEL and examining the influence of the additional stress produced by this expansion. Second, using the same model in a design capacity to assess the most beneficial expansion (or contraction) which a heat affected area may exhibit if it is to suppress crack growth, i.e. assuming that initiation of damage still occurs, how can a future rail material be created to suppress the growth of the initiated defect. A wheel running temperature of 300C is considered, separate to the prior severe thermal event [6].

2 MODELLING METHOD AND CONDITIONS

Modelling was conducted using a boundary element (BE) analysis in the Beasy software package [7] and considered cracks of 1mm to 15mm long, 1mm deep, parallel to the surface of a rail. This crack configuration was chosen as a simplified representation of the “stud” crack type shown in Figure 1. This type of crack is found in undeformed steel, and the crack sizes modelled were large relative to the microstructure dimensions, hence the model was of stress controlled crack growth, which was quantified by fracture mechanics. Microstructural anisotropy which would be important if there was extensive shear of the steel (typically affecting cracks much closer to the rail surface) was absent. The model (Figure 2) used a 2D plane strain representation of the rail-wheel contact, with a maximum

Hertzian contact pressure of 1014MPa. Surface and crack face friction coefficient was taken as 0.3, with a contact half-width of 5mm. This pressure and contact size correspond to a wheel of 780mm diameter and 6.5 tonne axle load running on a UIC60 rail worn to a slightly flatter than new condition crown radius. The 2D model was able to represent vertical and longitudinal stresses that characterise wheel motion in straight track, but could not represent the lateral forces or lateral crack growth that can be significant in curved track. This disadvantage was set against significantly lower solution times, enabling a wider range of conditions and crack sizes to be studied. The contact was taken to be fully sliding, with shear traction distribution across the contact defined by the product of Hertzian normal load distribution multiplied by friction coefficient. The conditions modelled are shown in Table 1. Metallurgical transformation of the pearlite to martensite was simulated on a macro scale through bulk expansion or contraction of the heat affected zone, not by modelling the thermo-mechanical behaviour of the microstructure itself. The expansion depends on the specific alloy composition of the steel, with two different cases considered in the paper alongside the ‘artificial’ contraction cases used for the design study.

2.1 Density based calculation of volume change

Values for the metallurgical transformation volume change of the heat affected area can be generated using either a density or an atomic volume based approach. To assess the change based on density, the density of pearlite was calculated by taking the density of its constituents ferrite (α iron, 7870 kg/m³) and cementite (Fe₃C, 7700 kg/m³) and their weight percentage, assuming a eutectoid composition steel with 0.77% carbon for which the weight fractions of ferrite to cementite are 8:1 [8]. This gives a density of pearlite with 0.77% C as 7851.1kg/m³, although this takes no account of the effect of other alloying elements on the density. The density of martensite is available from literature [9], although its value is sensitive to plastic deformation. This is particularly relevant to rail steel surfaces where plastic deformation of pearlite is common, although the increased hardness of martensite after transformation may protect it from further deformation. Density prior to plastic deformation [9] is 7790 kg/m³, but may drop to 7785 kg/m³ with 5% plastic deformation. Assuming the value for zero plastic deformation applies, the change from pearlite to martensite reduces density to $7790/7851.1 = 99.22\%$ through an expansion of 0.78% in volume. The expansion would be greater after plastic work. A value of 0.8% is used in Table 1 to capture this process.

2.2 Atomic volume change approach

An alternative to the bulk density based approach is to use atomic volume data for steel microstructures [10]. Taking carbon as a weight percentage (C) and atomic volume in Angstroms cubed, values are pearlite (11.916), austenite (11.401+0.329C), and martensite (11.789+0.370C). Considering a carbon fraction of 0.77% this indicates a change of atomic volume from 11.916 Å³ and 12.0739Å³ with the transformation from pearlite to martensite i.e. a volume expansion of just over 1.3%. Following similar reasoning the change from austenite to martensite is predicted to give an atomic volume increase of around 3.6%, which is in agreement with literature data for this transformation [11]. A value of 1.3% is used in Table 1 to capture this approach for the pearlite to martensite volume change.

2.3 Implementation of volume change in modelling

The exact value of volume change with transformation will depend on the steel chemistry, and also the exact thermal path taken as the steel is heated and cooled, but the methods outlined above gave a reasonable range for which modelling could be conducted to investigate the effect on cracks in a rail. To represent the expansion and contraction through transformation of a surface layer in the BE model a thermal body load was applied to the whole of the transformed layer (regardless of contact size or position) using a temperature calculated to achieve the required volumetric expansion [12]:

$$\frac{\Delta V}{V_0} = 3\alpha\Delta T \quad (1)$$

where $\Delta V/V_0$ is the volume change ratio, α is the thermal linear expansion coefficient for the material and ΔT is the temperature difference. It should be noted that this is simply a convenient way to implement expansion or contraction within an existing structure without modelling microstructural change or applying a mechanical load. It is an artificial temperature value, distinct from the thermal boundary condition applied to represent the passing of a hot wheel over the rail with which it is combined using superposition.

For the case with a rail-wheel contact temperature rise, it was assumed that the rail surface was heated in the wheel contact area, and was elsewhere at 20C. This was intended to simulate ‘flash’ heating of the rail surface followed by rapid cooling as the contact moves away. The properties of the rail steel were Young’s modulus, 210GPa, Poisson’s ratio, 0.3, and thermal linear expansion coefficient of 13 $\mu\text{m}/\text{mK}$. To identify the peak and range of stress intensity factors during the passage of a wheel, contact positions at 2.5mm increments were examined up to 15mm either side of the crack centre. No crack growth rate law exists specific to the loading and crack configuration used in the current investigation. Therefore, indicative crack growth rates were calculated using the lower bound method developed for inclined surface breaking cracks in rail steel [13, 14]. Although the crack configuration differs this growth law was generated using a normal grade rail steel and there is similarity in the combination of mode I and II loading for a crack under compression. A more specific growth law for modern rail steels would be a useful area of future research.

3 RESULTS & DISCUSSIONS

All the cases listed in Table 1 were investigated for a 1mm crack length to examine a crack which has already initiated but not yet grown significantly. Modelling was also performed for a range of crack lengths from 2 to 15mm but for economy of modelling these cases exclude conditions 4 and 5 (1.3% expansion due to transformation) since trends are visible from the baseline case and for $\pm 0.8\%$ expansion cases. For each condition modelled the range of stress intensity factor was assessed by considering the movement of a wheel incrementally across the crack (Figure 3), generating a series of SIFs. The combined action of traction and normal stress is indicated in the figure, and results in asymmetry of the results for left and right crack tips. Results are presented as stress intensity factors in Figure 4 to Figure 6, in which the origin is at the centre of the crack, hence crack tips will lie to the left or right of the origin according to crack size. Stress intensity factors are converted to indicative crack growth rates shown in Figure 7. As an addition to the SIF data, Table 2 shows stress calculated for a point 1mm below the centre of the contact and white etching layer region, but without a crack present. This indicates that thermal expansion is particularly influential on longitudinal stress, and to a lesser extent on lateral stress, while metallurgical transformation has a strong influence on longitudinal and vertical stress in the rail. These stresses are for just a single location, and it is their combination throughout the rail during passage of the wheel that determines the SIFs for each case considered.

3.1 Stress intensity factor dependence on crack size

Figure 4 shows the trends observed in K_I and K_{II} values for the left and right crack tips. These plots are for condition 1 (no expansion/contraction, no thermal input). For the left crack tip (Figure 4a), K_I shows a rise with increasing crack size, but is small even for a 15mm crack. For comparison a threshold stress intensity factor of 6 $\text{MPa}\cdot\text{m}^{1/2}$ for tensile growth of cracks in carbon steel is available from Otsuka et al. [15] and has been applied in previous work on crack growth in rail steel [16,17]. The mode II data for the left crack tip (Figure 4b) shows much larger stress intensity factor values, but a low sensitivity to crack size of the total range during passage of the contact. The values for shear mode growth comfortably exceed the 1.5 $\text{MPa}\cdot\text{m}^{1/2}$ shear mode threshold given by Otsuka et al. [15].

At the right crack tip both mode I and II SIF ranges show rising trends with increasing crack size (Figure 4c,d). The mode I values are very small, but the mode II values are comfortably above threshold. Assuming applicability of the crack growth law previously developed for inclined surface breaking cracks, Figure 7 and Table 3 show the outcome of mixed mode growth. There is a plateau in growth rate with increasing crack size for the left tip, but raising rates with increasing size at the right tip. This reflects similar trends in peak mode II SIF with increasing crack size for the left and right cracks (Figure 4b,d) and its strong influence over predicted crack growth rate. In crack growth for inclined surface breaking cracks it is thought that a small mode I crack opening stress (even if itself below threshold)

can “unlock” mode II growth through helping to overcome crack face friction [18]. In the current results high values of mode II are predicted even with almost zero K_I at the right tip, although larger K_I values are predicted at the left. This may influence the tendency of the right side crack to branch (the usual mode II growth behaviour), whereas prolonged co-planar growth may be possible with the higher mode I levels at the left tip. This is an aspect of the growth which requires further investigation, to better understand if and how the inclined surface breaking crack behaviour translates to these horizontal embedded cracks, and how they branch and propagate.

3.2 Effect of expansion and contraction of a thin surface layer

Figure 5 shows the effect on mode I and II stress intensity factor of expansion or contraction of a surface layer due to metallurgical transformation, focusing on just the 1mm length crack left tip. These data are generated without additional thermal stress as the wheel passes. Results for the right crack tip and at other crack sizes exhibit similar behaviour. The baseline case 1 is also included. Values of K_I rise well above the baseline when expansion of a thin surface layer is considered. Positive K_I values are present when the contact is absent, i.e. the crack becomes subject to a static mode I stress which is relieved as the compressive contact passes, producing a stress cycle. This is the case for the 1mm crack which is short relative to the 2mm transformed layer considered, but this effect diminishes as the crack exceeds the size of the transformed region. The values of K_I are low, in part because this is a small crack size, but they rise in proportion to the degree of expansion of the surface layer, representing possible reactions of different steel metallurgies (case 2 and 4, 0.8% and 1.3% expansion respectively). For the case of a 0.8% contraction of the surface layer (case 6) K_I is maintained at zero whatever the contact position.

For mode II under the same conditions moderate changes take place in the peak values determining stress intensity factor range during passage of the contact, but the overall form of the curves is similar for all cases. Inset graphs (Figure 5b) enable the order of the peak values to be identified. It can be seen that expansion of the surface layer increases the magnitude of both positive and negative peaks (dependent also on the level of expansion). Furthermore, contraction of the surface layer reduces the peak magnitudes, and hence the stress intensity factor range. Although the number of contact positions examined is limited, the relative size of the contact and crack mean the peak position is known in advance and can be accurately captured. The ranges can be seen numerically in Table 4. The changes are small, but when converted to crack growth rates (assuming applicability of the crack growth law), they raise or lower the crack growth rate relative to the baseline case across the range of crack sizes investigated, as indicated in Figure 7 and Table 3.

3.3 Effect of thermal input from passing wheels

Figure 6 shows a selection of cases to highlight the effect of additional thermal input from warm wheels passing a site of previous thermal damage with metallurgical transformation. Expansion and contract by 0.8% is considered, but the 1.3% cases are excluded from the plot for clarity. From Figure 6a for mode I it can be seen that the thermal input considered (dotted lines) makes insignificant changes to the stress intensity factor. The behaviour is dominated by the effect of metallurgical expansion relative to the base case (producing a rise in K_I values), or contraction (for which K_I is maintained at zero). As discussed above, the values of K_I are all very small, but it is the trends that are of significance.

For K_{II} (Figure 6b) the overall form of the curves for variation of stress intensity factor during the passage of the contact is insensitive to the differences between cases with and without additional thermal input. Dotted lines in the plot represent the cases with additional thermal input. At negative contact positions there is some sensitivity of K_{II} to thermal input. At positive contact positions there is almost no effect from thermal input, with K_{II} for metallurgical expansion or contraction cases being above or below baseline values irrespective of the additional thermal input.

The effect of thermal input on SIF range is shown numerically in Table 4. For both metallurgical expansion (cases 2, 3) and contraction (cases 6, 7) the trend emerges that thermal input produces (i) minor or no change in ΔK_I , and (ii) an increase in ΔK_{II} .

The crack growth predictions (Figure 7) show that a contracting microstructure is beneficial in suppressing crack growth (growth rate in case 6 is close to or reduced below the baseline case). However, this benefit is negated by surface heating from a warm wheel (case 7) for all but very small cracks which are wholly below the 2mm wide transformed expansion/contraction region. For an expanding microstructure (case 2) the crack growth rate is always above the baseline case, and is made even higher when a warm wheel is considered (case 3).

3.4 Microstructure design

The research presented in this paper has considered a range of crack sizes at 1mm below the surface, and indicates suppression of crack growth is possible if metallurgical transformation through thermal input produces contraction rather than expansion of the microstructure (considering this separately from temporary thermal expansion). This indicates it would be beneficial to study steel chemistry that can achieve this behaviour, or to undertake tests on a range of existing rail steels to see if some types already have this beneficial property. Beyond comparison of crack growth predictions with the physical evidence for existing rail defects (Figure 1), validation depends on identifying such a material, and developing a crack growth law specific to mixed mode non-inclined sub-surface cracks. When considering new rail coating technologies [19] there is also the possibility of choosing a coating with this crack suppressing property. Even if contraction cannot be achieved, there would be benefit in selecting steel metallurgy able to reduce levels of expansion when metallurgical transformation takes place following thermal input. In further work a crack closer to the surface will be considered to understand the very earliest stage in growth of a defect near thermal damage, and whether there is a prospect of “designing out” growth of cracks from this damage type.

4 CONCLUSIONS

Evidence of severe thermal loading (white etching layer, WEL) is often associated with rail defects. Severe thermal input has three main consequences, which last over different durations: (i) temporary thermal expansion of the steel, (ii) permanent metallurgical transformation of the steel to WEL, and (iii) permanent locked-in stress produced by the change of material volume associated with the metallurgical transformation. The modelling in this paper focuses on area (iii) and predicts that WEL can accelerate growth of cracks below it through locked in stress due to metallurgical transformation from pearlite to martensite which causes a local increase in volume of the rail steel. Conversely, taking a hypothetical case in which thermal damage leads to a permanent contraction of the steel microstructure it is predicted that crack growth rate can be reduced. The changes predicted in crack growth rate are small, but point to the interesting possibility that if a material (new steel chemistry or a clad layer of a non-steel material) were to contract locally in response to thermal damage it could suppress any subsequent crack growth close to this damage, or at the interface between the clad layer/repair and the underlying rail which is a crucial position prone to defects. Validation against physical samples depends on the creation of a suitable rail surface material offering contraction in response to thermal transformation. This, along with investigation to better understand if and how existing understanding of inclined surface breaking crack behaviour translates to horizontal embedded cracks, are the subject of future research.

ACKNOWLEDGEMENTS

The authors would like to thank SBB and Dr Stuart Grassie for initiating the project which led to this research. This research was supported by a scholarship from Universiti Tun Hussein Onn Malaysia (UTHM).

REFERENCES

1. Grassie S. L., Squats and squat-type defects in rails: the understanding to date, *IMechE J Rail Rapid Transit* 2012, 226, 235-242.
2. J. Ivanisenko, I. MacLaren, X. Sauvage, R. Valiev, H. Fecht, Phase transformations in pearlitic steels induced by severe plastic deformation, *Solid State Phenom.* 114 (2006) 133–144.
3. W.D. Callister, *Materials Science and Engineering: An Introduction*, John Wiley & Sons, New York, USA, 2007.
4. S. L. Grassie, D. I. Fletcher, E. A. Gallardo Hernandez, and P. Summers, Studs: a squat-type defect in rails, *IMechE. J. Rail Rapid Transit*, 226 (3) 243–256, 2011

5. D. I. Fletcher, Numerical simulation of near surface rail cracks subject to thermal contact stress, *Wear*, 314, 2014, 96–103
6. Cole, K. D., Tarawneh, C. M., Fuentes, A. A., Wilson, B. M., Navarro, L. (2010). Thermal models of railroad wheels and bearings. *International Journal of Heat and Mass Transfer*, 53(9), 1636-1645.
7. BEASY Boundary Element software. www.beasy.com. (Accessed 8th June 2016.)
8. V. Raghavan *Physical Metallurgy Principles and Practice*, 2012, PHI Learning Private Limited.
9. V. K. Sharma, N. N. Breyer, N. Abe, L. H. Schwartz, Effects of plastic deformation on the density of a medium carbon martensite, *Scripta Metallurgica*, Vol. 8, pp. 699-702, 1974
10. M. Narazaki, G. E. Totten, and G.M. Webster, *Handbook of Residual Stress and Deformation of Steel*. Ohio: ASM International, 2002, pp. 248–295.
11. J. M. Moyer and G. S. Ansell, The Volume Expansion Accompanying the Martensite Transformation in Iron-Carbon Alloys, *Metall. Trans.*, vol. 6A, pp. 1785–1791, 1975.
12. N. J. Giordano, *College Physics: Reasoning and Relationships*, 2010, Brooks/Cole Cengage Learning, 1st edition, pp 448.
13. P. E. Bold, M. W. Brown, and R. J. Allen, Shear mode crack growth and rolling contact fatigue, *Wear*, 144 (1–2), 307–317, 1991.
14. S. Bogdański, M.W. Brown, Modelling the three-dimensional behaviour of shallow rolling contact fatigue cracks in rails, *Wear*, 253 (1), 17-25, 2002.
15. A. Otsuka, K. Mori, T. Miyata, The condition of fatigue crack growth in mixed mode condition, *Eng. Fract. Mech.* 7 (1975) 429–439.
16. M. Kaneta, M. Suetsugu and Y. Murakami, Mechanism of Surface Crack Growth in Lubricated Rolling/Sliding Spherical Contact, *J. Appl. Mech.* 53(2), 1986, 354-360
17. Fletcher, DI, Beynon, JH, The effect of intermittent lubrication on the fatigue life of pearlitic rail steel in rolling-sliding contact, *Proceedings IMechE part F*, 214(3), 2000, 145-158
18. Bower, AF, The influence of crack face friction and trapped fluid on surface initiated rolling contact fatigue cracks, *Trans. ASME, J. Lubr. Technol* 110 (1988), pp. 704–711
19. S.R. Lewis, R. Lewis, D.I. Fletcher, Assessment of laser cladding as an option for repairing/enhancing rails, 20th International Conference on Wear of Materials, 12-16th April 2015, Toronto, Canada.

TABLES

| Case | Expansion due to transformation | Rail-wheel contact temperature rise / C |
|------|---------------------------------|---|
| 1 | 0 | 0 |
| 2 | 0.8% | 0 |
| 3 | 0.8% | 300 |
| 4 | 1.3% | 0 |
| 5 | 1.3% | 300 |
| 6 | -0.8% | 0 |
| 7 | -0.8% | 300 |

Table 1. Conditions modelled.

| Case | Longitudinal | Vertical | Lateral | Shear |
|------|--------------|----------|---------|--------|
| 1 | -661.2 | -995.6 | -497 | -209.1 |
| 2 | -632.8 | -968.7 | -480.5 | -212.5 |
| 3 | -604.4 | -965.1 | -470.8 | -213.2 |
| 6 | -688.9 | -1022 | -513.2 | -205.7 |
| 7 | -660.4 | -1018 | -503.6 | -206.5 |

Table 2. Stress (MPa) at 1mm from the rail surface, centrally below the contact and transformed layer.

| Case | 1 mm | | 2mm | | 5mm | | 10mm | | 15mm | |
|------|------|-----|-----|-----|------|-----|------|------|------|------|
| | L | R | L | R | L | R | L | R | L | R |
| 1 | 3.0 | 3.4 | 4.1 | 3.2 | 5.9 | 4.7 | 5.6 | 7.4 | 5.1 | 8.0 |
| 2 | 3.8 | 4.2 | 5.6 | 3.7 | 8.3 | 4.8 | 9.6 | 8.3 | 9.9 | 9.0 |
| 3 | 4.1 | 4.7 | 7.4 | 5.2 | 10.7 | 6.7 | 10.8 | 10.1 | 11.6 | 11.0 |
| 4 | 4.5 | 4.8 | - | - | - | - | - | - | - | - |
| 5 | 4.5 | 5.0 | - | - | - | - | - | - | - | - |
| 6 | 2.4 | 2.8 | 3.4 | 2.7 | 5.7 | 4.7 | 5.3 | 7.4 | 4.9 | 7.9 |
| 7 | 2.6 | 3.3 | 5.0 | 3.8 | 8.2 | 6.5 | 7.7 | 9.2 | 7.3 | 9.9 |

Table 3. Crack growth rates (nm/cycle) for all the cases and sizes of cracks modelled.

| Case | 1mm | | | | 2mm | | | | 5mm | | | | 10mm | | | | 15mm | | | |
|------|--------------|-----------------|--------------|-----------------|--------------|-----------------|--------------|-----------------|--------------|-----------------|--------------|-----------------|--------------|-----------------|--------------|-----------------|--------------|-----------------|--------------|-----------------|
| | L | | R | | L | | R | | L | | R | | L | | R | | L | | R | |
| | ΔK_I | ΔK_{II} |
| 1 | 0.1 | 14.2 | 0.1 | 14.8 | 0.2 | 15.6 | 0.0 | 14.4 | 2.6 | 17.3 | 0.3 | 16.3 | 4.2 | 16.7 | 0.3 | 18.7 | 4.4 | 16.1 | 0.3 | 19.2 |
| 2 | 1.4 | 15.1 | 1.2 | 15.6 | 2.2 | 17.0 | 1.7 | 15.0 | 3.4 | 19.1 | 1.5 | 16.3 | 5.5 | 19.5 | 2.2 | 19.3 | 6.2 | 19.5 | 2.9 | 19.7 |
| 3 | 1.3 | 15.5 | 1.2 | 16.3 | 2.1 | 18.6 | 1.7 | 16.7 | 3.4 | 20.7 | 1.5 | 18.1 | 5.6 | 20.3 | 2.1 | 20.5 | 6.3 | 20.6 | 2.8 | 21.0 |
| 4 | 2.1 | 15.7 | 1.9 | 16.1 | - | - | - | - | - | - | - | - | - | - | - | - | - | - | - | - |
| 5 | 2.1 | 15.8 | 1.9 | 16.3 | - | - | - | - | - | - | - | - | - | - | - | - | - | - | - | - |
| 6 | 0.0 | 13.3 | 0.0 | 13.9 | 0.0 | 14.7 | 0.0 | 13.7 | 2.4 | 17.1 | 0.8 | 16.3 | 4.1 | 16.4 | 0.7 | 18.7 | 4.4 | 15.9 | 0.5 | 19.1 |
| 7 | 0.0 | 13.6 | 0.0 | 14.6 | 0.0 | 16.6 | 0.0 | 15.3 | 2.2 | 19.2 | 0.6 | 18.0 | 4.2 | 18.5 | 0.5 | 20.0 | 4.6 | 18.1 | 0.3 | 20.5 |

Table 4. Mode I and II stress intensity factor range for all cases modelled.

FIGURE CAPTIONS

- Figure 1. Example of “stud” defect morphology below the running band in a longitudinal cross-section from a high speed mixed traffic line. The central portion of the crack is close to horizontal and lies at approximately 1mm below the rail surface in an undeformed microstructure. The white marker above the rail surface indicates the location of a patch of white etching layer on the rail surface. The surface depression and plastic deformation characteristic of a “squat” defect are absent.
- Figure 2. BE model of rail-wheel contact with horizontal crack of 1mm located 1mm below the rail surface. 2mm length of metallurgically transformed layer with 100 μ m thickness from a previous thermal event is shown grey. The heat source moves together with the contact load traversing the rail surface.
- Figure 3. A series of analyses are performed with incremental movement of the contact across the crack. The origin of the position is measured from the crack centre.
- Figure 4. Stress intensity factor dependence on contact position. (a) left tip mode I, (b) left tip mode II, (c) right tip mode I, (d) right tip mode II.
- Figure 5. Effect of metallurgical expansion and contraction (represented as density change) on stress intensity factor for 1mm crack, left crack tip. (a) Mode I, (b) mode II. Legend entries refer to cases in Table 1.
- Figure 6. Effect of additional thermal stress (warm wheels) on stress intensity factor for 1mm crack, left crack tip. (a) Mode I, (b) mode II. Legend gives case number from Table 1.
- Figure 7. Crack growth rate dependence on crack size for cases 1, 2, 3, 6, 7. (a) Left crack tip, (b) right crack tip. Case 6 is equal to the baseline case 1 for cracks of 5mm length and over.

FIGURES

Figure 1

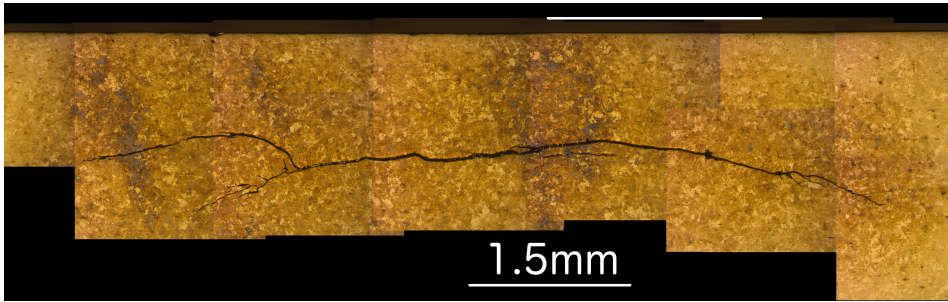


Figure 2

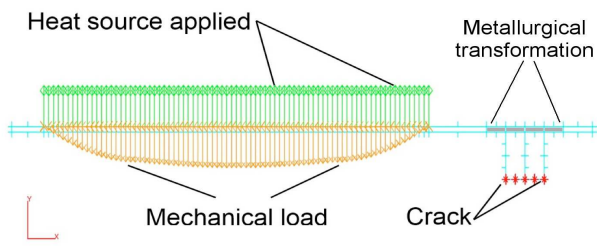


Figure 3

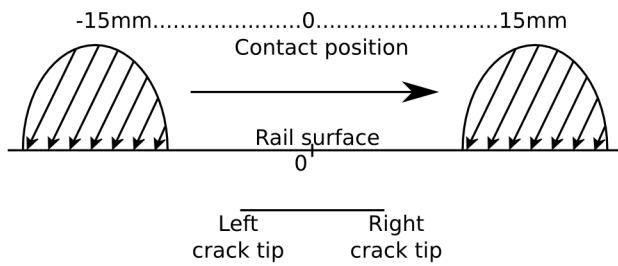


Figure 4a

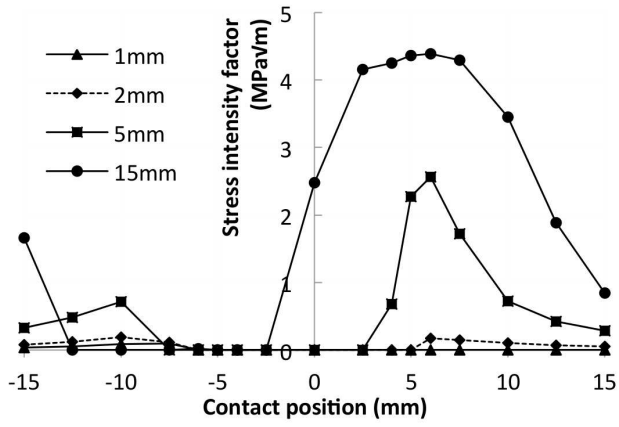


Figure 4b

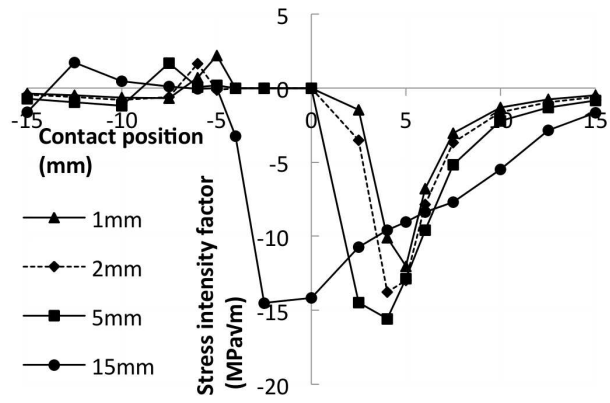


Figure 4c

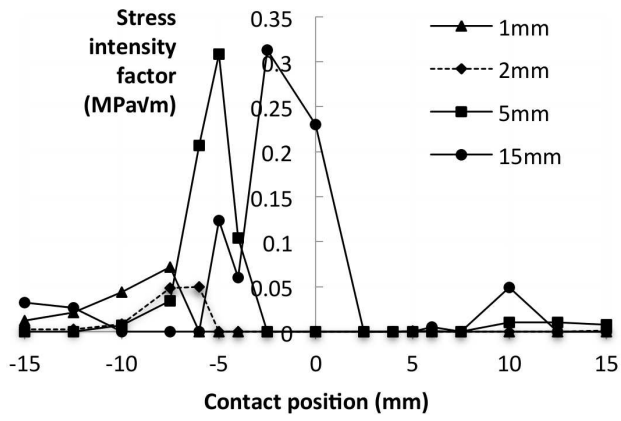


Figure 4d

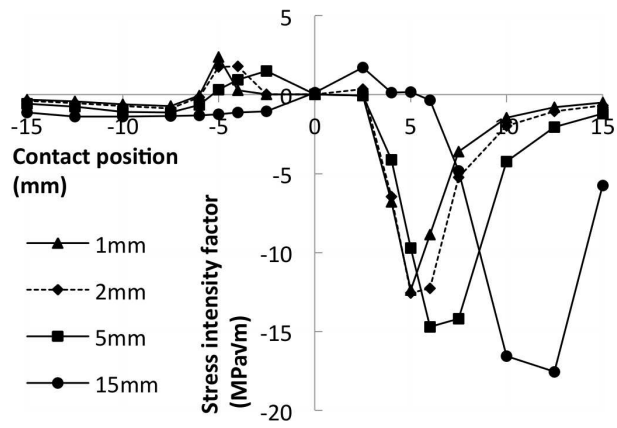


Figure 5a

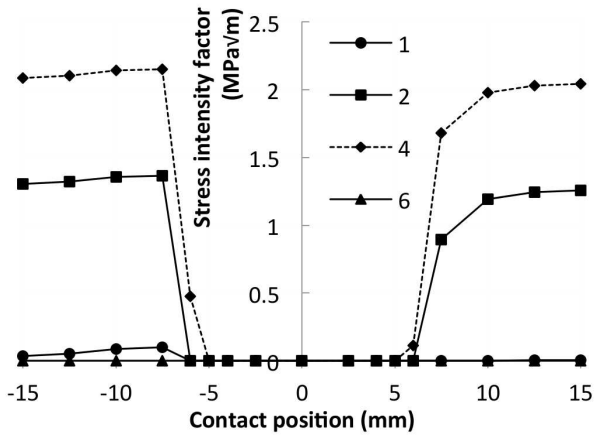


Figure 5b

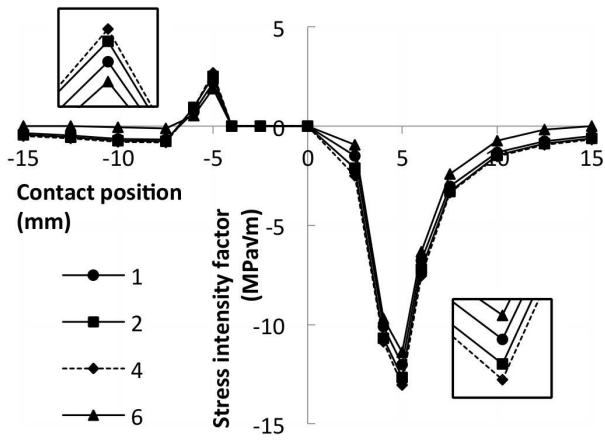


Figure 6a

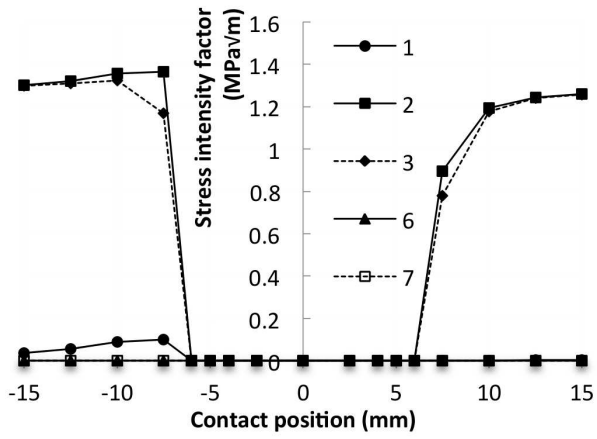


Figure 6b

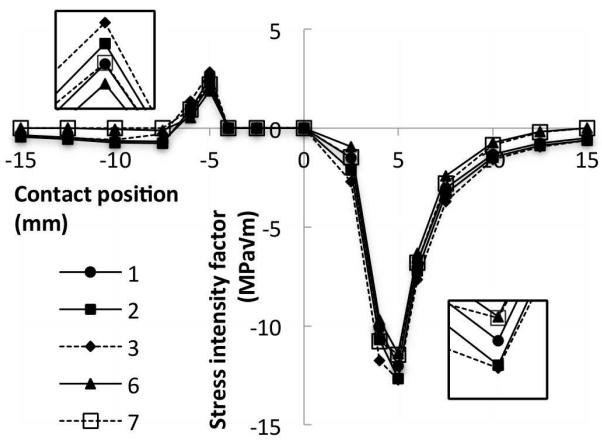


Figure 7a

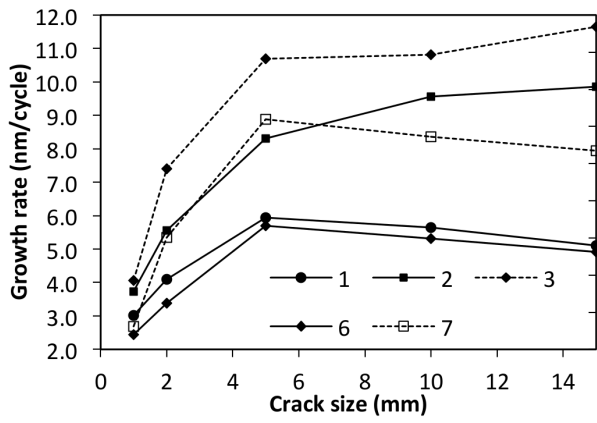


Figure 7b

